Design, Analysis and Control of a Semi-active Magnetic Bearing System for Rotating Machine Applications

T.-J. Yeh

Department of Power Mechanical Engineering, National Tsing-Hua University, Hsinchu, Taiwan, R.O.C.

Keywords: Magnetic Bearing, Permanent Magnet, LTR Control.

Abstract: In this paper, a semi-active magnetic bearing system which incorporates both the active and passive magnetic bearings is proposed for rotating machine applications. Particularly, the design, analysis, and control issues of the semi-active system are investigated by using an axial fan as the platform. In the proposed system, while the rotor is levitated axially by the active bearing, its radial and tilting stabilities are guaranteed by the passive bearings. By carefully designing the radial and tilting stiffnesses of the passive bearings and the controller of the active bearing, the system can be successfully operated to the rated speed of $4000rpm$. Because the semi-active magnetic system is frictionless and consumes insignificant power in levitation, its total power consumption is 14.7% less than the conventional fan in which mechanical ball bearings are used.

1 INTRODUCTION

The use of magnetic bearings in industrial applications has attracted increasing attention in recent years. The major advantage offered by magnetic bearings is that there is no physical contact between the bearing and the levitated object, so friction is eliminated and lubrication is not needed. In general, magnetic bearings can be classified into two types: the active type and the passive type. Active magnetic bearings are made of electromagnets whose coil currents are controlled based on the sensor measurements(T.-J. Yeh and Wu, 2001)(Yeh et al., 2001). Active magnetic bearings allow the system designers to flexibly adjust the bearing stiffness and damping, and inject appropriate signals to cancel the undesired vibrations. Nevertheless, due to the necessary control hardware including sensors, control electronics/digital signal processor, and power amplifiers, the use of active magnetic bearings substantially increases system cost and complexity. On the other hand, passive magnetic bearings are simply made of permanent magnets and rely on either the attractive or repulsive magnetic force to achieve levitation (J. Delamare and Yonnet, 1995)(H. Okuda and Ito, 1984)(Yonnet, 1981). Passive magnetic bearings do not require any control hardware as the active bearings do, so they are inexpensive and structurally simple. However, by Earnshaw's theorem, total stability is not possible for systems containing only passive magnetic bearings. In these systems, the object to be levitated always has to be constrained mechanically in certain degrees of freedom. As a result, physical contact is established and frictional loss is induced.

Considering the pros and cons in magnetic bearings, if one wants to keep the system complexity to minimum and yet achieve total levitation, the most economical solution will be a system combining the favorable features from both types of the bearings, or so-called the semi-active magnetic bearing system. Semi-active systems have been reported by several researchers. For example, in (J. Delamare and Rulli, 1994) an angularly stable radial bearing is incorporated with an active magnetic bearing in the axial direction to levitate a rotor. However, due to the low stiffness in the passive bearing, total levitation is not possible for the whole range of speed that the rotor has to start its rotation with ball bearings until the first critical speed of $750rpm$ is passed. In (J.F. Antaki and Groom, 2000)(J.F. Antaki and Groom, 2001), the authors devised a magnetically levitated blood pump as the artificial heart. In this system, the rotor is suspended by two permanent magnet radial bearings and an active magnetic thrust bearing which is actuated by two voice coils. With the help of the blood as the damping source, the system is capable of spinning between $4000rpm$ and $8000rpm$. In this paper, the development of a semi-active magnetic bearing system for rotating machine applications is demonstrated by using a commercially available $127mm \times$

Yeh T..
Design, Analysis and Control of a Semi-active Magnetic Bearing System for Rotating Machine Applications.
DOI: 10.5220/0005528205030510
In *Proceedings of the 12th International Conference on Informatics in Control, Automation and Robotics* (ICINCO-2015), pages 503-510
ISBN: 978-989-758-122-9

$127mm \times 38mm$ axial fan as the platform. The axial fan, whose photograph is shown in Figure 1, is driven by a brushless DC motor and uses axial air flow to provide cooling for computer peripherals. Given the limited space for mounting the magnetic bearings, the requirement to spin to the rated speed of $4000rpm$ without using any mechanical bearings, as well as lack of fluid damping because the fan is operated in the air, the development requires systematic procedures in design, analysis, and control. The rest of the paper is organized as follows: System configuration and dynamic analysis of the semi-active magnetic bearing system are introduced in section 2. Section 3 discusses how the passive bearings are designed to achieve the desired radial and tilting stiffnesses. In section 4, the physical model of the active magnetic bearing is first presented. Then system identification and controller design are performed to stabilize the bearing dynamics. Section 5 presents experimental verifications of the system performance. Finally, conclusions are given in section 6.

Figure 1: Photo of the axial fan.

2 SYSTEM CONFIGURATION AND DYNAMIC ANALYSIS

Figure 2 shows the schematic of the semi-active magnetic bearing system. There are one active magnetic bearing and two passive magnetic bearings. The active bearing consists of an annular electromagnet and a thrust disk which contains a circular permanent magnet with the same diameter as the inner pole face of the electromagnet. This active bearing is used to provide frictionless support to the rotor in the axial direction. Since feedback is always needed for the active bearing, a fiber-optic sensor, which measures rotor's axial position, is mounted on a structural member whose both ends are in turn attached rigidly to the top of the fan housing.

Passive bearing I is composed of two permanent magnet rings with one on the top of the rotor and the other attached to the same structural member on which the senor is mounted. The two magnets are polarized axially and are aligned with the rotor's axis. Because the magnets are placed in attractive manner, an upward magnetic force is applied to the rotor. Passive bearing II consists of two concentric stacks of permanent magnet rings respectively attached to the rotor and the housing. The permanent magnet rings are polarized axially and are stacked in a repelling manner for squeezing more magnetic fluxes towards the air gap between the stacks. The polarities of the two stacks are arranged so that they repel against each other. Moreover, because the magnetic poles of the outer stack are not aligned with those of the inner stack, passive bearing II applies an downard force to the rotor. These two sets of passive bearings together serve two purposes. One is to provide tilting and radial stiffnesses so that when the rotor tilts or translates radially, a restoring torque or force can be produced. The other is to provide a suitable upward axial bias force for the active bearing to counteract. Such a counteraction allows the active bearing, which generates downward force only, to have full control of rotor's axial motion so as to generate axial stiffness.

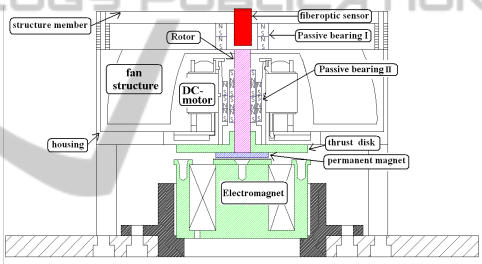

Figure 2: Configuration of the semi-active magnetic bearing system.

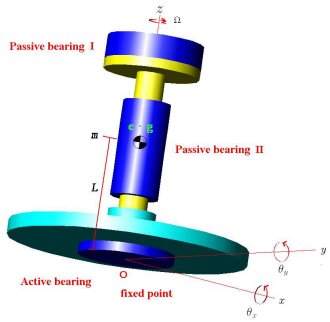

Figure 3: Definitions of variables for dynamic analysis.

The dynamic analysis follows the definitions of variables in Figure 3. For simplification, it is assumed that the controller of the active magnetic bearing renders the rotor with high axial stiffness that the center point of the thrust disk, or the point O in Figure 3, can be treated as a fixed point in the free space. By doing so, the rotor becomes an axially symmetric body spinning about a fixed point. The rotor dynamics is

thus given by:

$$\begin{aligned} m\ddot{x} + k_r x &= me\Omega^2 \sin\Omega t \quad (1)\\ m\ddot{y} + k_r y &= me\Omega^2 \cos\Omega t \quad (2)\\ I_t\ddot{\theta}_x + \Omega I_a\dot{\theta}_y + (k_\theta - mgL)\theta_x &= me\Omega^2 L\sin\Omega t \quad (3)\\ I_t\ddot{\theta}_y - \Omega I_a\dot{\theta}_y + (k_\theta - mgL)\theta_y &= me\Omega^2 L\cos\Omega t \quad (4)\end{aligned}$$

where m is the mass of the rotor, I_t is the transverse moment of inertia about the fixed point, I_a is the axial moment of inertia, Ω is the rotor speed, x, y and θ_x, θ_y are respectively the rotor's radial displacements and tilting angles, k_r and k_θ are the radial and the tilting stiffnesses provided by the magnetic bearings, L is the distance from rotor's center of gravity to the fixed point O, and e is the rotor unbalance. It should be noted that while the first two equations are from the translational dynamics, the last two are due to the gyroscopic effect. Moreover, the right side of the equations are caused by the unbalance forces (torques) which are proportional to $me\Omega^2$ and are synchronized with Ω.

By considering the resonance in the rotor dynamics, one can compute the minimum bearing stiffnesses needed for the rotor to successfully spin to the rated speed of $4000rpm$. Taking the the radial stiffness k_r for example, in order to avoid resonance during acceleration of the rotor, it is desired to place the resonant frequency above the rated speed. For $m = 0.2kg$ and the given rated speed, it can be shown from (1) or (2) that k_r has to be larger than $35,092\frac{N}{m}$. The rotor in consideration has a mass unbalance specification of $85\mu m$. If keeping the amplitude of vibration within $0.25mm$(which equals half of the bearing gap) at the rated speed is desired, then the lower bound for k_r is raised to $47,000\frac{N}{m}$. To determine the tilting stiffness, by taking Laplace transform on (3) and (4), it can be found that if $k_\theta > mgL$, the rotor is stable with two resonant frequencies:

$$\omega^2_{n1,n2} = \frac{1}{2I_t^2}\left\{\left[2I_t(k_\theta - mgL) + \Omega^2 I_a^2\right] \pm\sqrt{\Omega^4 I_a^4 + 4I_t(k_\theta - mgL)\Omega^2 I_a^2}\right\} \quad (5)$$

Figure 4 shows how ω_{n1}, ω_{n2} (in the unit of rpm) vary with for $I_a = 1.4\times10^{-4}kg\cdot m^2$, $I_t = 3\times10^{-4}kg\cdot m^2$, $L = 0.022m$, and $k_\theta = 1,\ 8,\ 18.02\frac{N\cdot m}{rad}$. Apparently, while ω_{n1} increases with Ω, ω_{n2} decreases with Ω. When either one of the resonant frequencies equals the rotation speed, resonance occurs. Ideally, to avoid the resonance as Ω varies from zero rpm to the rated speed, the two resonant curves should not intersect with the $\omega_n = \Omega$ line in Figure 4. It can be computed that to achieve such a condition k_θ has to be greater than $55\frac{N\cdot m}{rad}$.

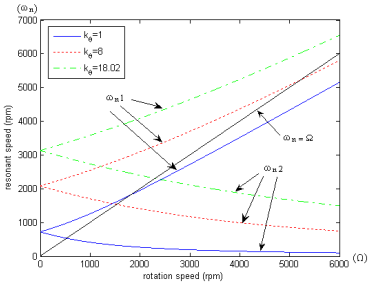

Figure 4: Resonant speed v.s. rotation speed for different.

3 DESIGN AND ANALYSIS OF PASSIVE MAGNETIC BEARINGS

Although the lower bounds for the radial and tilting stiffnesses can be computed via the dynamic analysis, it is still desired to make the stiffnesses as high as possible for minimizing rotor's vibration during spinning. However, as implied by Earnshaw's theorem, the stable radial and tilting stiffnesses simultaneously induce instability in the axial direction and indeed the instability increases with the stable stiffnesses. In sizing the passive bearings, other than pursuing high radial and tilting stiffness, the axial instability also has to be kept low so that the active bearing is able to compensate.

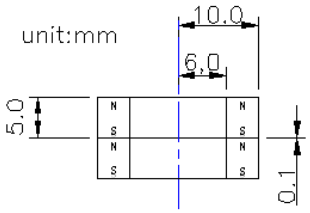

Figure 5: Schematics of Passive Bearing I.

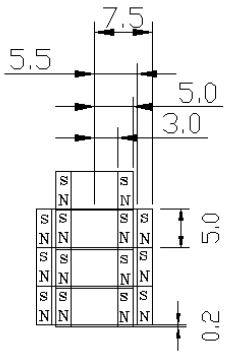

Figure 6: Schematics of Passive bearing II.

In this research, a finite-element package(ans,) is employed to analyze the relevant bearing proper-

ties including stiffnesses and instabilities so that a better compromise among the design parameters can be achieved. The magnetic material used here is NdFeB with the remanence magnetic flux density of $1.23Telsa$. The schematics of two passive bearings obtained after several design iterations are shown respectively in Figure 5 and Figure 6. Particularly, in passive bearing II, while the outer stack consists of three magnetic rings, the inner stack consists of four magnetic rings, and the magnetic poles of the outer stack are dislocated from those of the inner stack by $0.2mm$ in the downward manner.

Table 1: Properties of the Passive Bearings.

	Passive Bearing I	Passive Bearing II
Radial Stiffness	$8,000\frac{N}{m}$	$38,000\frac{N}{m}$
Tilting Stiffness	$16.62\frac{N\cdot m}{rad}$	$1.4\frac{N\cdot m}{rad}$
Axial Instability	$26,300\frac{N}{m}$	$74,400\frac{N}{m}$
Axial bias force	$49.44N$	$-21.2N$

The radial stiffness, tilting stiffness, axial stability and the upward force respectively provided by the two passive bearings are listed in Table 1. According to this table, the tilting stiffness is mainly contributed by passive bearing I and the radial stiffness is mainly contributed by passive bearing II. In order to keep the axial instability to minimum, we deliberately limit the radial stiffness of passive bearing II, which is the main source of axial instability, to $38,000\frac{N}{m}$ by having unequal numbers of magnetic rings for the inner and outer stack[1]. The total radial stiffness in this case is only $46,000\frac{N}{m}$, which is still $1,000\frac{N}{m}$ less than the lower bound computed in previous section. As will be shown later, the additional radial stiffness needed will be provided by the active bearing. From the table it can also be found that the total tilting stiffness is only $18.02\frac{N\cdot m}{rad}$, which means that the rotor will experience a resonance at $2,200rpm$. Due to the limited space for placing the magnets and the unavailability of magnets of extreme strength, it is difficult to further increase the tilting stiffness to avoid the resonance. In the following investigation, this tilting stiffness is adopted, so as the rotor accelerates towards the rated speed, it will experience resonance shortly. Since the unbalance force is small at low speeds, as long as the rotor accelerates fast enough, it will not collide with the stator and such resonance will be acceptable. Finally, the dislocation between the concentric stacks of bearing II induces a downward axial bias force of $21.2N$ to the rotor. This downward force is used to cancel part of the upward force from bearing I. By doing so, the total upward force that the active bearing has to counteract is not excessive and thus its power consumption at steady state is reduced.

[1]The finite element simulations indicate that if the inner and outer stacks of passive bearing II both have three rings, then the radial stiffness is only $33.450\frac{N}{m}$. If the number of rings for both stacks are increased to four, the radial stiffness becomes $44,510\frac{N}{m}$ but the axial instability also becomes excessive. As a comprimise, unequal number of rings are adopted respectively for the outer (3) and inner (4) stack.

4 MODELING, IDENTIFICATION, AND CONTROL OF THE ACTIVE MAGNETIC BEARING

In the active magnetic bearing, if the magnetic flux leakage, fringing flux, and the magnetic reluctance in the iron core are ignored, one can derive the following magnetic force equation:

$$F_m = \frac{-A_2\left[\mu_0 Ni + B_r l/\mu_r\right]^2}{2\mu_0(z+l/\mu_r)^2(1+A_2/A_1)} \quad (6)$$

where F_m is the downward magnetic force generated, μ_0 is the air permeability, μ_r and B_r are respectively the relative permeability and the remanence magnetic flux density of the permanent magnet, z is the air gap, μ_0 is the air permeability, i is the coil current, N is the number of coil turns, l is the thickness of the permanent magnet, A_1 and A_2 are respectively the areas of the inner(circular) and outer(annular) pole faces. Table 2 lists the numerical values of the relevant parameters for the active magnetic bearing. Comparing the magnetic force computed by (6) with the finite-element simulations, it can be found that the theoretical equation tends to overestimate the magnetic force because it ignores the magnetic flux leakage and fringing flux associated with the permanent magnet. To make a more accurate force prediction, one can introduce a correction factor η in which ηl replaces l in (6) as the equivalent thickness of the permanent magnet. By choosing η to be 0.946, Figure 7 shows that the theoretical equation matches the finite element results better with maximum error less than 3%.

4.1 Linear Model and Identification

To facilitate the subsequent linear control design, the nonlinear force equation (6) with the correction factor is linearized around $i = 0$, and $z = z_0$, where z_0 is the nominal air gap. The linearization results in

$$F_m \approx -k_i\delta i + k_s\delta z - F_b \quad (7)$$

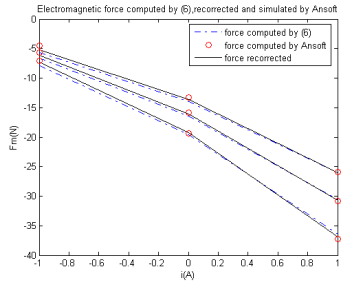

Figure 7: Comparisions of the force equations with the finite-element results.

Table 2: The numerical values of the relevent parameters for the active magnetic bearing.

A_1	$3.14\times10^{-4}\ (m^2)$
A_2	$7.06\times10^{-4}\ (m^2)$
μ_0	$4\pi\times10^{-7}$
N	$300\ (turn)$
B_r	$0.55\ (T)$
l	$2\times10^{-3}(m)$
μ_r	1.06

where $k_i = \frac{A_2 N B_r \eta l/\mu_r}{(z_o+\eta l/\mu_r)^2(1+A_2/A_1)}$ is the current gain, $k_s = \frac{A_2[B_r\eta l/\mu_r]^2}{\mu_0(1+A_2/A_1)(z_o+\eta l/\mu_r)^3}$ is the unstable stiffness, $F_b = \frac{A_2(B_r\eta l/\mu_r)^2}{2\mu_0(z_0+\eta l/\mu_r)^2(1+A_2/A_1)}$ is the downward bias force provided by the permanent magnet, δi and δz denote the perturbations in current and axial displacement respectively. If z_0 is selected to be $0.2mm$, then $F_b \approx 21.385N$. This bias force, when combined with the rotor's weight, cancel most of the upward force from the passive bearings. Therefore, if the active bearing is stabilized at this nominal air gap, the steady-state power required for levitation is insignificant.

It should be noted that although the active bearing is open-loop unstable in the axial direction, it is stable in the radial and tilting directions. Finite element simulations reveal that the associated radial and tilting stiffnesses are respectively $1,000\frac{N}{m}$ and $0.01\frac{N\cdot m}{rad}$. Although the tilting stiffness is minuscule compared to those offered by the passive bearings, as mentioned in the previous section that such a radial stiffness is just enough to limit rotor's amplitude of vibration to within half of the airgap as the rotor accelerates towards the rated speed. Assume that the passive bearings' downward force balances with the rotor's weight and permanent's bias force, the linearized dynamic equation for the axial motion can be derive as

$$m\frac{d^2z}{dt} = (k_s + k_p)z - k_i i \qquad (8)$$

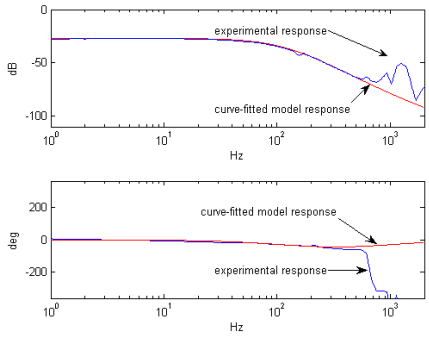

Figure 8: Frequency responses of the active magnetic bearing.

where k_p is the total axial instability contributed by the two passive bearings. Notice that in this equation the perturbation symbol δ associated with i and z has been removed for simplicity. By substituting the respective numerical values into (8) and then taking Laplace transform, the system transfer function $G(s)$ can be computed as

$$G(s) = \frac{z(s)}{i(s)} = \frac{-11.9}{0.2s^2 - 114,000} \qquad (9)$$

System identification is performed on the active bearing to experimentally identify the transfer function. The identification is based on frequency response tests. Because the system is open-loop unstable, the identification is performed in closed loop by using a PID controller to stabilize the system. During the identification test, a sinusoidal signal, whose frequency ranges from $10Hz$ to $10kHz$, is injected as a disturbance and the frequency response is obtained by comparing the amplitudes and phases of the coil current and the rotor position.

In Figure 8, the experimental frequency response is shown. This frequency response is also curve-fitted by a transfer function which retains the form of the theoretical input-output behavior in (9) except that one extra pole and zero are added. The transfer function, given by

$$G(s) = \frac{z(s)}{i(s)} = \frac{-10(\frac{s}{5027}+1)}{(0.21s^2 - 100,000)(\frac{s}{942}+1)} \qquad (10)$$

is also plotted in Figure 8. The second order part of this transfer function, which has phase of zero for all frequencies, only differs slightly from the theoretical model, and the extra pole and zero added are used to account for the additional phase lag for $\omega > 10Hz$. It should be noted that the experimental frequency response matches the curve-fitted transfer function except for the first structural frequency at about $200Hz$ and other structural modes occurring at $\omega > 500Hz$. Therefore, the transfer function in (10) will be used

as the nominal model and its discrepancy from the experimental frequency response will be treated as the modeling error in the following controller design.

4.2 LTR Controller Design

The PID controller designed for identification, although is simple and stabilizing, has limited performance due to its restricted control structure and trial-and-error nature. Experimentally, the axial stiffness provided by the PID controller is too compliant for the rotor to spin. In this section, we use the loop-transfer-recovery (LTR) design to systematically devise a high-performance controller to increase the stiffness of the active bearing.

In order for the control system to be stiff enough to reject disturbances at low frequencies, an integrator is augmented to $G(s)$ and then the LTR design is conducted on the state-space representation of the augmented system. LTR is a linear quadratic Gaussian (LQG) optimal control based method. The design procedure requires one to solve two algebraic Riccati equations: one corresponds to the Linear Quadratic Regulator problem, and the other to the Kalman Filter problem. As shown in (Athans, 1986), by implementing the cheap control LQR problem in LQG, the system's loop transfer function can be recovered to a Kalman filter loop transfer function which mimics a pure integrator with a bandwidth equal to $\frac{1}{\sqrt{\mu}}$, where μ is a fictitious output noise intensity. This indicates that the LTR design allows one to designate the closed-loop system bandwidth by the choice of μ.

Ideally the closed-loop bandwidth should be set as high as possible so that the system can achieve better disturbance rejection. However, the higher the bandwidth, the less likely the control system can maintain the robust stability against the modeling error. To select the appropriate bandwidth, we employ the small-gain result (K. Zhou and Glover, 1996) which, when applied to the current case, states that given a nominal model G with additive modeling error ΔG, a stabilizing controller K can provide robust stability if

$$|\Delta G(j\omega)| < \left|(1+K(j\omega)G(j\omega))^{-1}K(j\omega)\right|. \quad (11)$$

Figure 9 plots $\left|(1+K(j\omega)G(j\omega))^{-1}K(j\omega)\right|$ corresponding to several different designated bandwidths as well as $|\Delta G(j\omega)|$ which denotes the modeling error between G and the experimental frequency response in Figure 8. It is clear that when ω_b is raised to $60Hz$, the two functions in (11) intersect with each other at the first structural frequency. Thus in the final LTR design $\omega_b = 50Hz$ is adopted and the controller is given by

$$K_{LQG}(s) = -\frac{8.23\times10^9 s^3 + 1.358\times10^{13}s^2 + 5.635\times10^{15}s + 1.602\times10^{17}}{s(s^4 + 9224s^3 + 4.157\times10^7 s^2 + 1.147\times10^{11}s + 1.621\times10^{14})} \quad (12)$$

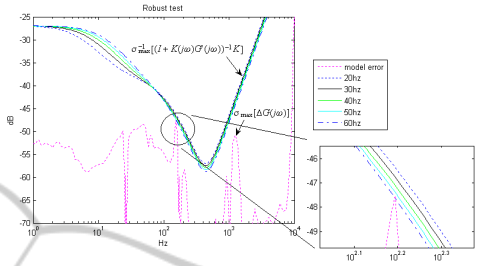

Figure 9: Examination of robust stability criterion in the frequency domain.

5 EXPERIMENTS AND PERFORMANCE EVALUATION

Figure 10 shows the photo of the semi-active magnetically-levitated axial fan for experimental validation. To initiate the levitation, the LTR controller is demanded to track a 2nd-order critically damped trajectory so that the rotor can eventually settles at the nominal gap. The displacement response in Figure 11 indicates the controller can inhibit the transiency to within 0.3sec. According to the current response in Figure 12, to achieve so the maximum coil current is less than $2.5A$. Moreover, the steady-state current is less than 0.1A, which implies that the active bearing consumes almost zero power for levitation. It should be noted that this steady-state current can be further reduced by slightly modifying the designated nominal air gap.

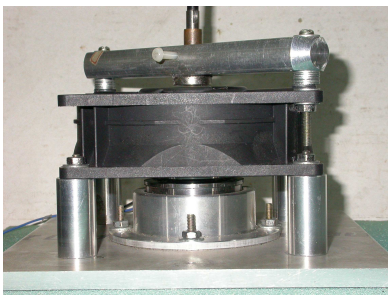

Figure 10: Photo of the semi-active magnetically levitated axial fan.

When the rotor is levitated axially by the active bearing, its radial and tilt stabilities are also automatically guaranteed by the passive bearings. After the rotor settles to the nominal gap at steady state,

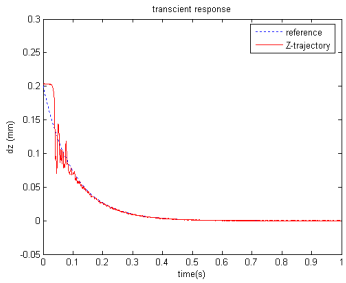

Figure 11: Transcient response of the axial displacement.

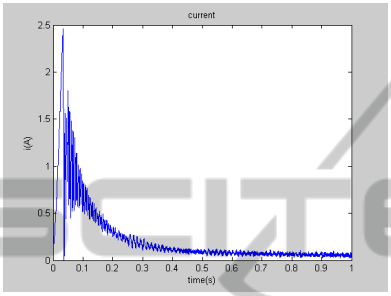

Figure 12: Transcient response of the coil current in the active magnetic bearing.

the brushless DC motor is activated to spin the rotor. The spinning test indicates that the rotor can spin successfully to $4000rpm$. Figure 13 shows the disturbance rejection responses of the active bearing for $0rpm$, $2000rpm$, and $4000rpm$. The experimental setup for identifying these responses is the same as what used in system identification except that the input is changed to the disturbance signal. This figure indicates that the LTR controller renders the active bearing fairly consistent disturbance-rejection performance as the rotor speed varies. Particularly, the static axial stiffness is greater than $10^7 \frac{N}{m}$, which verifies the high stiffness assumption in section 2. The amplitudes of axial vibration and radial vibration[2] for different spinning speeds are respectively shown in Figure's 14 and 15. It is clear that the bearings can limit the rotor's vibration to within one tenth and half of the bearing gap respectively in axial and radial directions. Moreover, according to Figure 15 the radial vibration is most significant between $2000rpm$ and $3000rpm$. This verifies the previous calculation on the gyroscopic resonant frequency associated with the designated tilting stiffness $18.02 \frac{N \cdot m}{rad}$.

The radial vibration of the semi-active magnetically levitated fan is also compared with two other systems. One is the original fan in which mechanical ball bearings are used to support the rotor, and the other is the passive magnetic bearing system whose

[2] The radial vibration is measured experimentally using a laser displacement sensor.

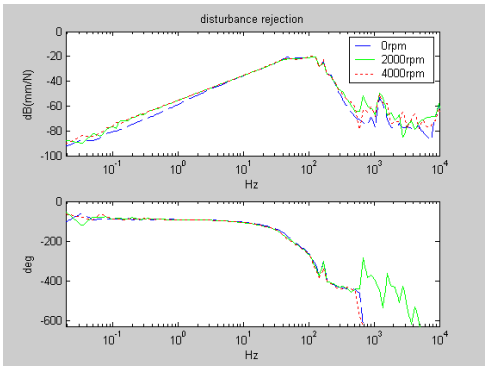

Figure 13: Disturbance rejection responses of the active magnetic bearing.

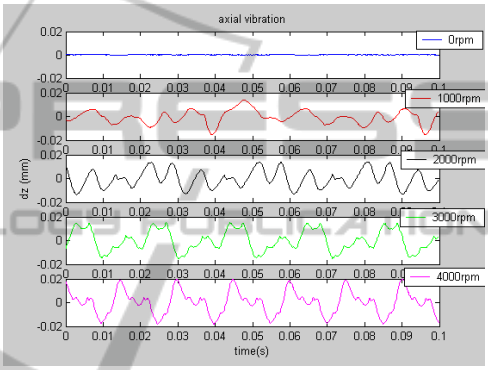

Figure 14: Steady state response of the axial displacement.

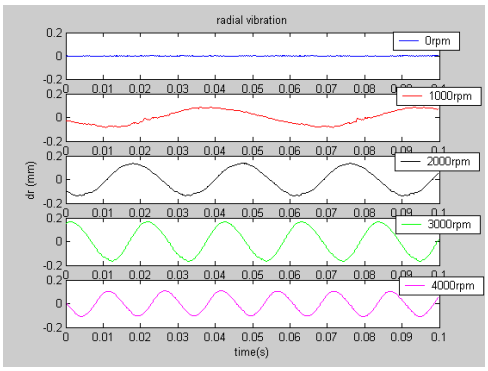

Figure 15: Steady state response of the radial displacement.

structure is similar to the current one except that the active bearing is replaced by a mechanical thrust bearing. The results of comparison are shown in Figure 16. Due to the gyroscopic resonance, the semi-active system exhibits highest amplitude of vibration between $1000rpm$ and $3000rpm$. After $3000rpm$, the semi-active system's vibration becomes smaller than the passive one but still larger than the original fan. In general, the vibration of the original fan is the lowest among the three systems for $\Omega > 1000rpm$. The power consumption of these three systems are also experimentally compared and the results are plotted in

Figure 17. It should be noted that while the power in the semi-active system is consumed by the DC motor and the active bearing, the power for the other two systems is solely consumed by the motor. As shown in this figure, because the semi-active system is totally frictionless and consumes almost zero-power in levitation, it exhibits the lowest power consumption among the three systems. Particularly, at the rated speed the semi-active system consumes 14.7% less than the original fan and 12% less than the passive bearing system.

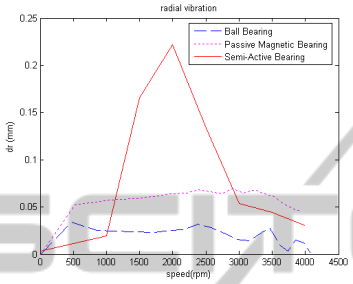

Figure 16: Comparision of the radial displacement for three systems

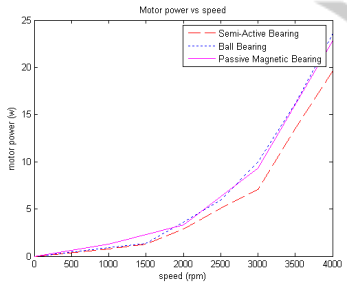

Figure 17: Comparison of power for the three systems

6 CONCLUSIONS

In this paper, a semi-active magnetic bearing system which incorporates both the active and passive magnetic bearings is proposed to support the rotor of an axial fan. By carefully designing the radial stiffness and tilting stiffness of the passive bearing and the controller of the active bearing, the system can be successfully operated to the rated speed with less power consumption than the original fan. Currently, two research efforts are conducted to further improve the proposed system. One is to use inexpensive, small hall-effect sensors to replace the expensive, bulky fiber-optic sensor for positioning sensing. The other is to modify the design of passive bearing I so that it can be integraged with passive bearing II and be placed internally. By doing so, the structural member which mounts the magnetic ring and the senor can be removed and the size, weight as well as the cost of the semi-active system can be reduced.

ACKNOWLEDGEMENTS

The author gratefully acknowledges the support provided by Ministry of Science and Technology of Taiwan.

REFERENCES

Ansoft corporation, maxwell 3d, pittsburgh, pa, 2003.

Athans, M. (1986). A tutorial on the lqg/ltr method. In *Proc. American Control Conference*, Seattle, WA.

H. Okuda, T. Abukawa, K. A. and Ito, M. (1984). Characteristics of ring permanent magnet bearing. *IEEE Transactions on Magnetics*, MAG-20(5).

J. Delamare, E. R. and Yonnet, J.-P. (1995). Classification and synthesis of permanent magnet bearing configurations. *IEEE transactions on Magentics*, 31(6).

J. Delamare, J.-P. Y. and Rulli, E. (1994). A compact magnetic suspension with only one axis control. *IEEE transactions on Magentics*, 30(6).

J.F. Antaki, B. Paden, G. B. and Groom, N. (2000). Magnetically suspended miniature fluid pump and method of designing the same.

J.F. Antaki, B. Paden, G. B. and Groom, N. (2001). Blood pump having a magnetically suspended rotor.

K. Zhou, J. D. and Glover, K. (1996). *Robust and optimal control*. Prentice Hall.

T.-J. Yeh, Y.-J. C. and Wu, W.-C. (2001). Robust control of multi-axis magnetic bearing systems. *International Journal of Robust and Nonlinear Control*, pages 1375–1395.

Yeh, T.-J., Chung, Y.-J., and Wu, W.-C. (2001). Sliding control of magnetic bearing systems. *ASME Journal of Dynamic Systems, Measurement*, 123(3):353–362.

Yonnet, J.-P. (1981). Permanent magnet bearings and couplings. *IEEE transactions on Magentics*, 17(1).